

Influence of friction stir processing on mechanical properties and the microstructure of aluminum-silicon cast alloys

Alaa Mohammed Hussein Wais^{1,*}, Jassim M.Salman Ahmed², Ouda Al-Roubaiy³

¹Biomedical Engineering Department, College of Engineering and Technology, Al-Mustaqbal University, 51001 Hillah, Babil, Iraq.

^{2,3}Metallurgical Engineering Department/College of Materials, Engineering/University of Babylon, Iraq

Received 22 Oct 2024

Accepted 22 Dec 2024

Abstract

Aluminum-silicon alloy castings can benefit from friction stir processing (FSP) locally. In this work, the result of FSP on sand castings of aluminum-silicon cast alloys 4%, 12% and 15% Si was investigated. The influences of different processing parameters on the microstructure and mechanical properties include the rotation speed (560, 710, 900 rpm) and the transverse speed (86, 189, 393) mm/min. Various tests of mechanical, including impact, micro hardness and tensile tests, have been carried out. An infrared (IR) camera fitted by software to evaluate the image of thermal for the treatment zone and ascertain the temperature at particular locations was used to investigate the temperature distribution. Results suggest that increasing rotational speed leads to an increase in heat generation, whereas increasing transverse speed leads to a decrease in heat generation. Hardness measurements were carried out throughout the entire process zone, Tests for tensile strength were conducted at room temperature, and FSP resulted in very little change in the hardness while significantly improving its properties of tensile and impact. The cast aluminum-silicon alloys' microstructure significantly improved after FSP. Nevertheless, differences in microstructure were noted throughout the processed zone, with the advancing side typically having a more refined and distributed microstructure than the retreating side. The best speeds (rotating speed of tool (710 rpm) and speed of transverse (189 mm/min) that gave best results.

© 2025 Jordan Journal of Mechanical and Industrial Engineering. All rights reserved

Keywords: Anodizing, Mechanical properties, Microstructure, Friction stir processing.

1. Introduction

Friction stir processing is a processing method developed by Mishra and Mahoney [1]. The Welding Institute (TWI) in the United Kingdom created the principles of friction stir welding (FSW) in 1991 with the aim of developing surface and local properties at specific locations. By using the friction stir welding concept, it is possible to create new processes because it is characterized by its special properties, which include high plastic material flow, low heat generation and an extremely fine grain size in the stirring area. Therefore, a general technique for changing the microstructure and composition at specific locations is the friction stirring process [1]. In addition, a surface composite was created on an Al substrate via the FSP technique [2], as were metal matrix composites, cast aluminum alloys and powder metallurgy (PM) aluminum alloys [3]-[4]. Owing to their excellent castability, high-temperature resistance and attractive density. However, increasing engine efficiency requires increasingly harsh operating conditions, meaning that the performance of existing materials must be improved. The large deformation caused by the movement of a rotating welding tool is used in FSP to refine the microstructure of a range of materials. [5]-[6]-[7]-[8]-[9]. Studies on the

application of FSP have shown that it can lead to a high degree of particle refinement in the second phase and a decrease in the size of the grains [10]-[11]. The fatigue properties and high-temperature mechanical performance of cast Al-Si alloys should be improved by fine-tuning their microstructure [12]-[13]. Al-Si alloys are widely used in automotive applications (Automotive Pistons) and Electrical industry [14]-[15]-[16]. In this work, the effects of (FSP) parameters on the mechanical properties and microstructures of Al-Si alloys are experimentally investigated.

2. Experimental Work

The influence of FSP on microstructure and the mechanical properties of aluminum-silicon alloys was investigated in this study. Hardness, impact strength and tensile strength tests were conducted to determine the mechanical properties of the material before and after FSP. During this study, eutectic Al-4 wt% Si, eutectic Al-12 wt% Si and eutectic Al-15.5 wt% Si alloys were used as the materials for the friction stir processing experiments. Table 1 shows the chemical analysis results for each of these alloys.

* Corresponding author e-mail: ...

Table 1. Chemical compositions for the three silicon casting alloys used in the experiments.

Alloy	Elements(wt%)		
	Si	Fe	AL
#1	4.23	0.16	Bal.
#2	12	0.23	Bal.
#3	15.55	0.24	Bal.

Commercially pure Al (99.7%) and commercially pure silicon (Si-99.96%) were melted separately in a clay-bonded graphite crucible. The melt was kept at 900 °C and continuously mixed using a graphite mixer up until the aluminum melt contained all of the silicon.. Sand mold casting is a method used in the casting process for each of these alloys. The plate was formed as a 200 × 130 mm plate with a thickness of 14 mm, which was left unchanged as a cast. The material was cooled in air to room temperature; as a result, the surfaces of the panels were uneven and rough because of casting shrinkage and uneven cooling. An X12 alloy steel tool was used to conduct the friction stir processing experiment. This steel is used in tool and bearing applications. Table 2 shows the chemical composition for X12 tool. Figure 1 shows a list of tool geometry details.

Table 2. Chemical composition (wt%) of the X12 tool.

C%	Cr%	Mn%	Si%	Fe%
2.00	11.5	0.30	0.34	Rem.

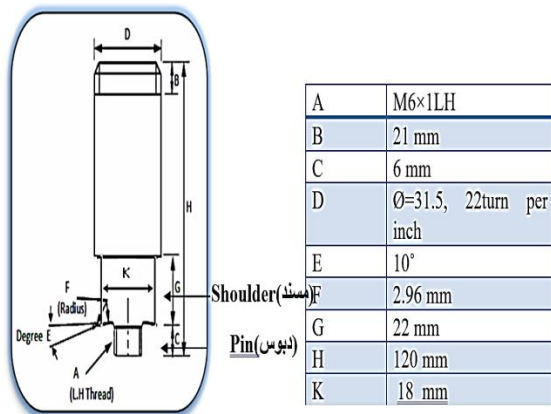


Figure1. Details of the tool geometry.

Investigations were conducted effects FSP on various aluminum-silicon cast alloys by varying the rotational and transverse speeds. Table 3 shows the FSP conditions applied to each alloy.

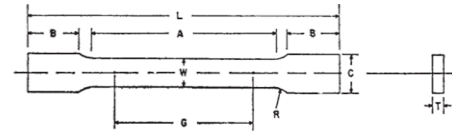
Table 3. FSP-specific processing parameters.

Alloy	Transverse Speed (mmmin ⁻¹)	Speed of Rotation (rpm)		
		560	710	900
#1	86	*	*	*
	189	*	*	*
	393	*	*	*
#2	189	*	*	*
#3	189	*	*	*

Microstructure test: Commonly used metallographic techniques were used to prepare the samples. The end

result of this process was a flat, smooth surface with no scratches.

Tensile test: Tensile samples were manufactured via a vertical milling machine in accordance with ASTM B 557 M-02a; the sample geometry was optimized (see Figure 2). From these tests, the tensile strength and elongation were calculated via a universal testing machine (see Figure 3) [17].



Symbol	Sub size specimen 6mm wide
G-gage length	25±0.1
W-width	6.01±0.05
T-thickness	5
R-radius of fillet, min	6
L-overall length, min	100
A-length of reduced section, min	32
B-length of grip section, min	32
C-width of grip section, approximate	10

Figure 2. Campione Subdimension Standard ASTM for test tension.



Figure 3. Universal test machine.

Impact Test: Using an instrumented pendulum machine, impact tests were performed on machined samples (FIT-300 N). Undersized Charpy V samples (10 × 5 × 55 mm) with a 2 mm deep V-notch conform to ASTM E23.

Hardness Test: Microhardness testing is a simple and quick method. Therefore, the method was applied to record the hardness profiles of the FSP samples throughout the machined zones. Measurements were taken at the sites in accordance with ASTM E3841, with readings taken every 1 mm. There was a load of 200 g and a load duration of 20 seconds.

Measurement of the temperature distribution: The main factor in determining the changes in microstructures and properties in the nugget zone and the heat-affected zone is the heat generated during FSP. During FSP, the temperature points in the plates were measured via an infrared (IR) camera.

X-ray Diffraction: was used to identify the alloys before FSP (XRD).

3. Results and Discussion

3.1. Analysis of the grain structure.

Prior to FSP, casting microstructures of all alloys were extremely coarse, as shown in Figure 4. The “grains” found in the hypoeutectic alloy were overall coarser than those in the eutectic and hypereutectic alloys. This occurred because the higher Si content of the eutectic and hypereutectic alloys altered the solidification pathway and promoted primary Si and eutectic cell nucleation and growth rather than primary α -Al phase. Additionally, owing to the faster cooling rate, the grains that formed closest to the plate surfaces were also finer than the grains that formed in the center of the material. Since Alloy-3 contains more Si than Alloy-2 does, compared to Alloy-2, its eutectic cells are finer [18].

3.2. Morphology of the individual phase

Silicon: Figure 4 shows the high volume proportion of Si particles in all three alloys. Both eutectic and primary Si particles were present in (Alloy-2 and Alloy-3), whereas the hypereutectic alloy Alloy-1 contained only eutectic Si[2]. Primary Si is observed in the microstructure as regularly faceted rhombohedral particles at low cooling

rates [19]. On the other hand, eutectic Si can form flakes or fibers depending on chemical modification and the cooling rate. Si flakes were found in all three alloys because of their comparatively slow rate of cooling. Figure 4. In general, the Si particles in the alloys became coarser as the distance from the cast plate surface increased. The reason for this is that the material near the surfaces cools faster than the material in the middle. This gives the center more time for growth and a lower nucleation rate. Figure 5 shows that the morphology and size of the eutectic Si flakes were comparable in all alloys. The majority of particles for primary Si developed in clusters within Alloy-3 (Figure 5c).

3.3. Grain Refinement during FSP

3.3.1. Influence of FSP on Hypoeutectic alloys.

Figure 6 shows and compares optical micrographs of the cast material with those of advancing and receding sides of process zone (PZ) in the midplane. As previously reported by other authors [15, 18, 20], FSP significantly refined the microstructure of this alloy (alloy 1). Consequently, a noticeable reduction in dimensions can be observed, and during the FSP process, the revolving instrument effortlessly breaks the coarse eutectic particles and Si flakes [15, 21].

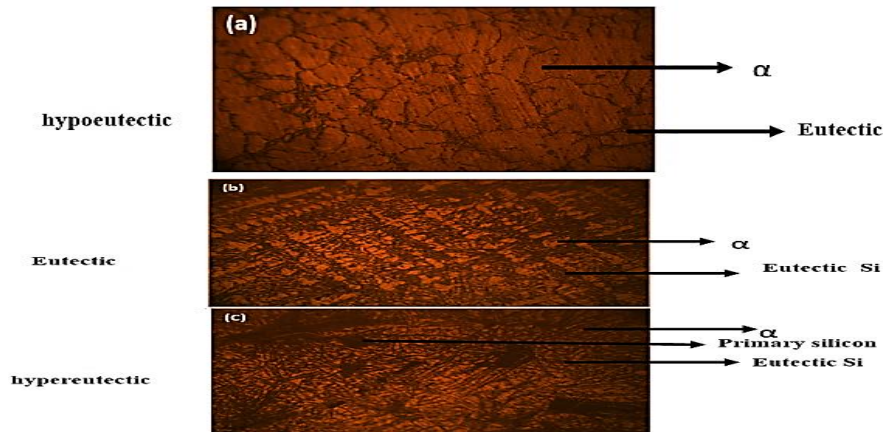


Figure 4. Optical images of the casting microstructures (a)alloy-1, (b)alloy-2 and (c)alloy-3 samples before FSP (400X).

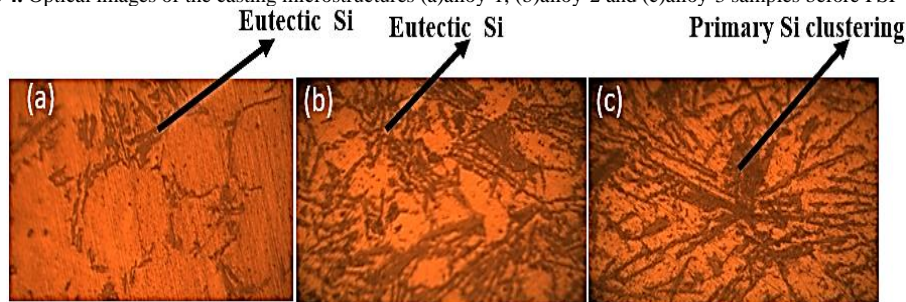


Figure 5. Optical image of (a) Si eutectic flakes in alloy-1, (b)Si eutectic flakes in alloy-2, (c)Si primary clustering in alloy-3 (400X).

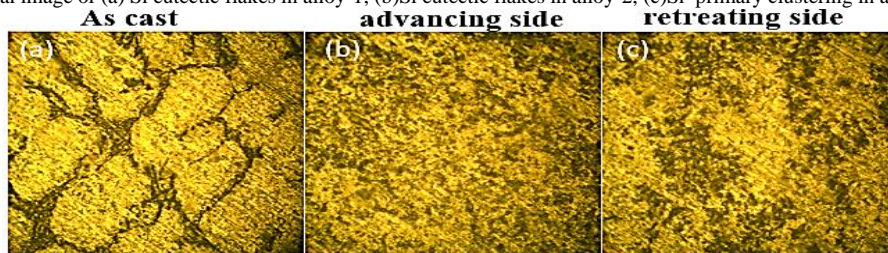


Figure 6. Optical image of the (a) Alloy-1 casting microstructure (b) side of the advancing and (c) side of retreating after FSP at a rotation speed of 710 rpm and speed of 189 mm/min (400X)

Figure 7a shows a picture of this PZ generated by FSP at a rotation rate of 710 rpm and a transverse speed of 189 mm min⁻¹, with important areas highlighted. The PZ has several distinguishable characteristics. First, there is a unique area of extremely fine microstructure directly under the tool shoulder. The grain size distribution within this thin layer of the surface is homogeneous and fine (Figure 7b). The “flow arm” is the material that has been pulled from the less deformed TMAZ across the weld

and into the PZ, as further shown in Figure (7c). In contrast, the particles at the retreat edge exhibited a wider transition region, as shown in Figure (7d), where the size change was more gradual [1,22].

The refined grains on the forward side of process zone were finer and more uniform than those on the retreat side. Figure (7) shows the finer distribution of the particles along the feed side. However, as one approaches the boundary of the process zone, the grains gradually increase

in size to the size of the grains in the starting material. The reason for this is that the grains were less evenly distributed and coarser from the centerline of the PZ to its retreat side (see Figure 6)

3.3.2. Influence of friction stir processing on the eutectic and hypereutectic alloys

Images (8 and 9) depict the common refined microstructures found in the process zone (Alloys-2 and 3) following Friction stir processing. In addition to a minimal increase in the particle concentration, this increase is attributed to the higher Si content of the alloys, and there appear to be no significant differences in the refined grain microstructures of the hypoeutectic alloy compared with those of the eutectic and hypereutectic alloys. However, the primary Si particles that dissolved initially had a smaller particle aspect ratio and were initially much larger.

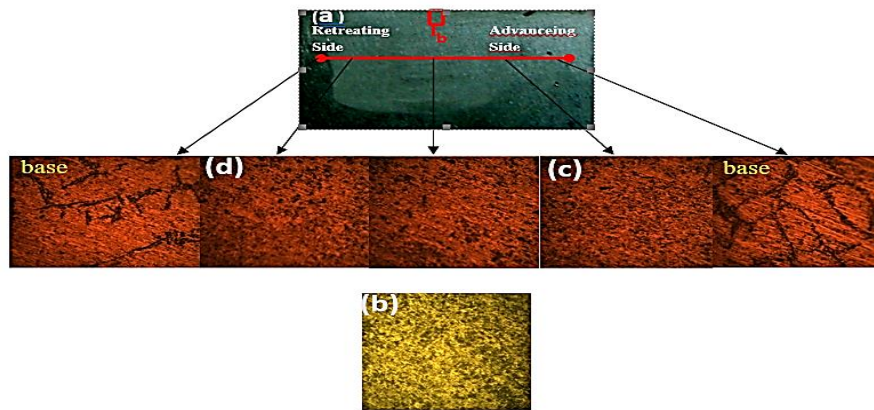


Figure 7. (a) An image illustrating the key properties of an Alloy-1 PZ fabricated with a rotational speed of 710 rpm and a transverse speed of 189 mm/min. (b) Refined surface layer; (c) advancing side; and (d) retreating side is visible at high optical magnification (400x).

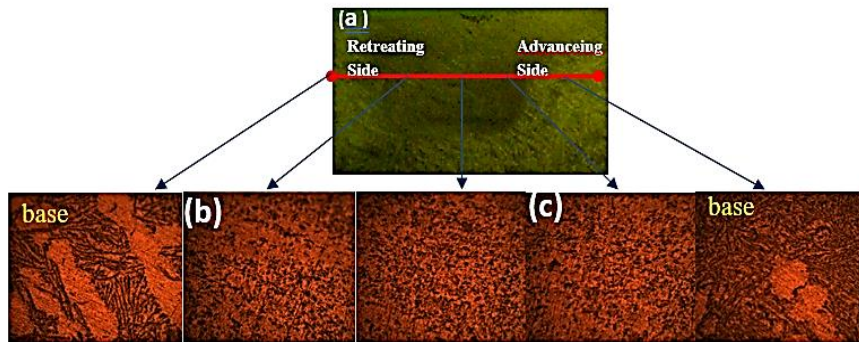


Figure 8. (a) An image illustrating the main characteristics of a normal PZ (Alloy-2) manufactured with a rotation speed of 710 rpm and a transverse speed of 189 mm/min. High optical magnification (400x) shows (b) side of the advancing and (c) side of the retreating.

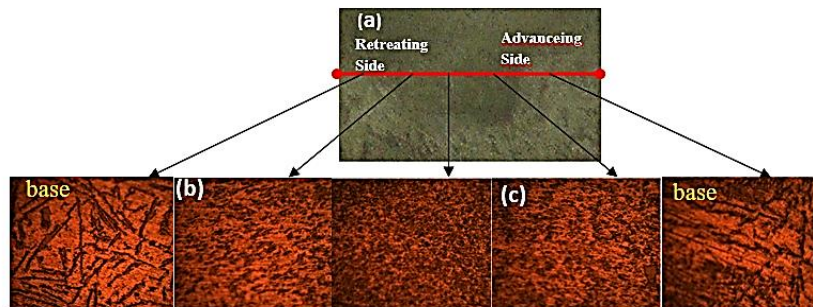


Figure 9. (a) An image illustrating the main characteristics of a normal PZ (Alloy-3) manufactured with a rotation speed of 710 rpm and a transverse speed of 189 mm/min. High optical magnification (400x) shows (b) side of the advancing and (c) side of the retreating

3.3.3. Effects of FSP parameters on changes in the PZ geometry and in the cross section.

Processing parameters changed in the PZ geometry and in the cross section, attached to pin, as shown in Figure 10. At low speeds, the PZ adopted the traditional “basin” geometry with a significant amount of material affected by FSP. In contrast, increased rotational speed led to the development of a “tube-like” structure. The volume of the PZ decreased and the deformation was more pronounced in the pin and shoulder area. The conversion to processes zone form is a result of the changed material flow dynamics during FSP, which in turn, as rotation speed increases, the material's peak temperature rises. It is believed that the postmaterial interaction adopts “adhesive behavior” at low processing temperatures [23, 24].

3.4. Tensile test results

Tables (4-6) present the tensile test results. The average results of the three tests are shown. The properties for tensile of the as-cast alloys frightened. Tensile profiles of Alloy-1 over the PZ as examples. Alloy-1 clearly had a mean tensile strength (UTS) of 87 MPa and a total elongation to failure of 8.8%. The tensile properties of the alloy significantly improved immediately after FSP. Mainly by removing pores and refining the microstructure, the tensile strength could be increased to over 140 MPa, and the ductility could be increased to over 20%. According to research by other scientists, the tensile properties of Al-Si cast alloys improve as the density and size of the pores decreases[25]. Notably, compared to the material processed at 560 rpm, the sample treatment at 710 rpm seemed to have better qualities. This discrepancy is most likely caused by the processing temperature of the material during FSP. The strength can increase because of the higher peak processing temperature at high rotation speeds [26].

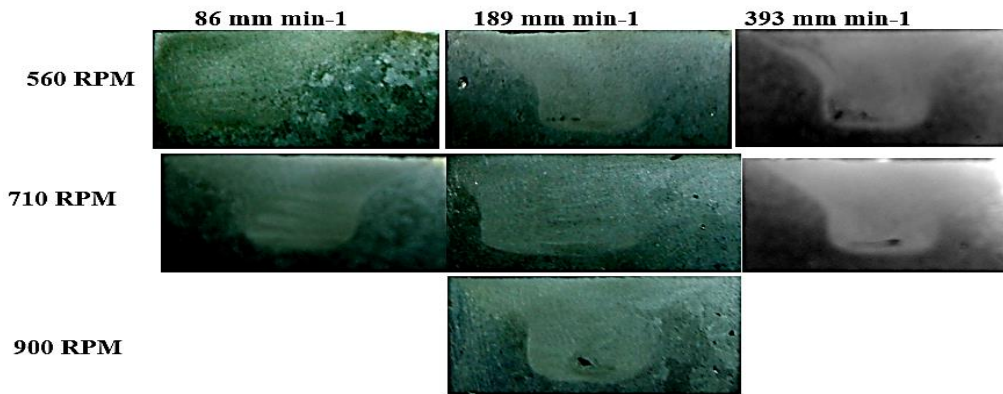


Figure 10. Images illustrating how the rotational speed and transverse speed affect the crosssection of the FSP zone(IX).

Table 4. Results of the tensile tests for Alloy-1.

Number of Sample	Rotating Speed of Tool (rpm)	Speed of Transverse (mm/min)	Strength of Tensile (MPa)	Strength of Yield (MPa)	Elongation (%)
AS CAST			87	71	8.8
AS FSP1	560	86	132	92	16
AS FSP2	710	86	116	85	16
AS FSP3	900	86	93	81	11.2
AS FSP4	560	189	142	90	19.8
AS FSP5	710	189	143	73	21.4
AS FSP6	900	189	117	91	19.2
AS FSP7	560	393	108	80	12.3
AS FSP8	710	393	139	100	19.7
AS FSP9	900	393	125.5	104	14.5

Table 5. Results of the tensile tests for Alloy-2

Number of Sample	Rotating Speed of Tool (rpm)	Speed of Transverse (mm/min)	Strength of Tensile (MPa)	Strength of Yield (MPa)	Elongation (%)
CAST			124	107	6
FSP1	560	189	133	86	15
FSP2	710	189	161	90	15
FSP3	900	189	666	57	7

Table 6. Results of the tensile tests for Alloy 3.

Number of Sample	Rotating Speed of Tool (rpm)	Speed of Transverse (mm/min)	Strength of Tensile (MPa)	Strength of Yield (MPa)	Elongation (%)
AS CAST			84	83	2.5
AS FSP1	560	189	141	78	12.1
AS FSP2	710	189	157	95	12.2
AS FSP3	900	189	127	87	10.3

3.5. Impact test results

Tables (7-9) list the Charpy impact test results (average values from three tests) for the three alloys. According to the results, the impact energy of the friction stir processed material (11 J) (AS FSP4) (710 rpm, 189 mm/min) was greater than that of the corresponding base metal (1.3 J) for Alloy-1. Impact energy from (0.5 J) to (5.3 J), (AS FSP1) (189 mm/min, 560 rpm) for Alloy-2. Impact energy from (1 J) to (5 J) for Alloy-3, (FSP1) 189 mm/min, 560 rpm. The impact energy is shown in Figures (11-13). This sharp increase in the total absorbed impact energy is due to the FSP-induced microstructural changes in the recrystallization of the process zone dynamics and the grain refinement, which eliminate the work hardening effect.

The lateral velocity effect is another observation of the impact results. As the transverse velocity increased, and decrease of the absorbed energy because of slow softening rate of the treatment. Furthermore, the reduction in absorbed energy is the result of an increase in rotational speed, similar to [18].

Table 7. Impact test results for the Alloy-1 FSP sample

Number Specimen	Rotating Speed (RPM)	Transverse Speed (mm/min)	Absorbed Energy (Joule)
AS CAST	-----	-----	1.3
AS FSP1	560	86	8.2
AS FSP2	710	86	7.3
AS FSP3	900	86	3
AS FSP4	560	189	11
AS FSP5	710	189	7
AS FSP6	900	189	5
AS FSP7	560	393	10.2
AS FSP8	710	393	6.1
AS FSP9	900	393	3.7

Table 8. Impact test results for the Alloy-2 FSP samples

Specimen Number	Rotating Speed (RPM)	Transverse Speed (mm/min)	Absorbed Energy (Joule)
AS CAST	-----	-----	0.5
AS FSP1	560	189	5.3
AS FSP2	710	189	4.6
AS FSP3	900	189	2

Table 9. Impact test results for Alloy-3 FSP samples.

Specimen Number	Rotating Speed (RPM)	Transverse Speed (mm/min)	Absorbed Energy (Joule)
AS CAST	-----	-----	1
AS FSP1	560	189	5
AS FSP2	710	189	2.4
AS FSP3	900	189	1.5

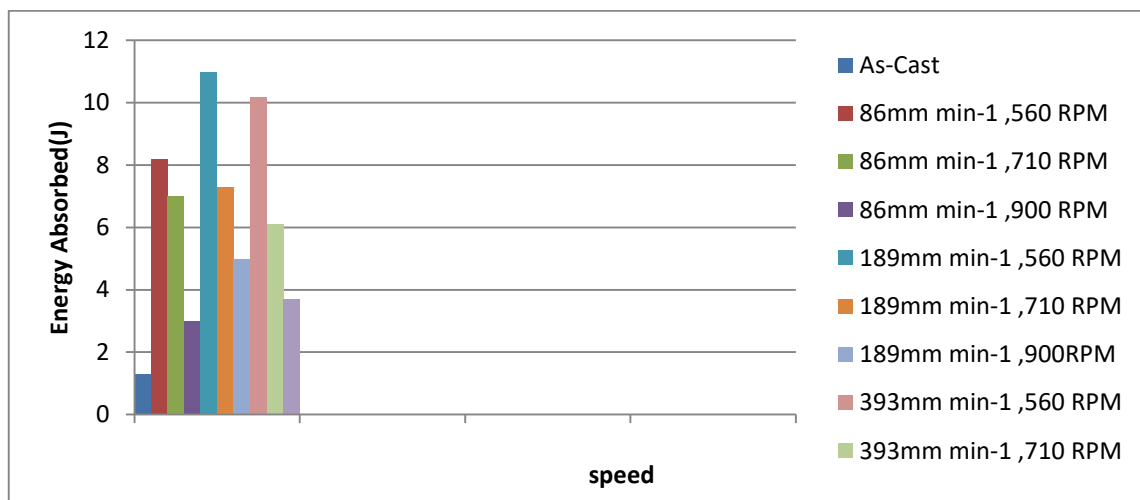


Figure 11. The impact energy absorbed by the PZ of Alloy-1 after FSP depends on the rotational and transverse speeds of the tool.

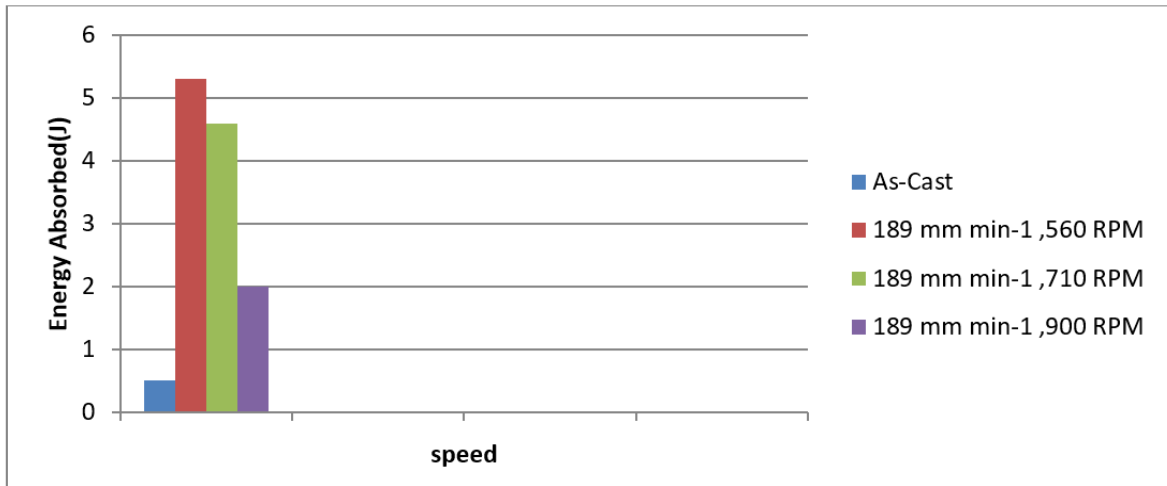


Figure12. Impact energy absorbed by the PZ for Alloy-2 to FSP depends of tool rotation speed.

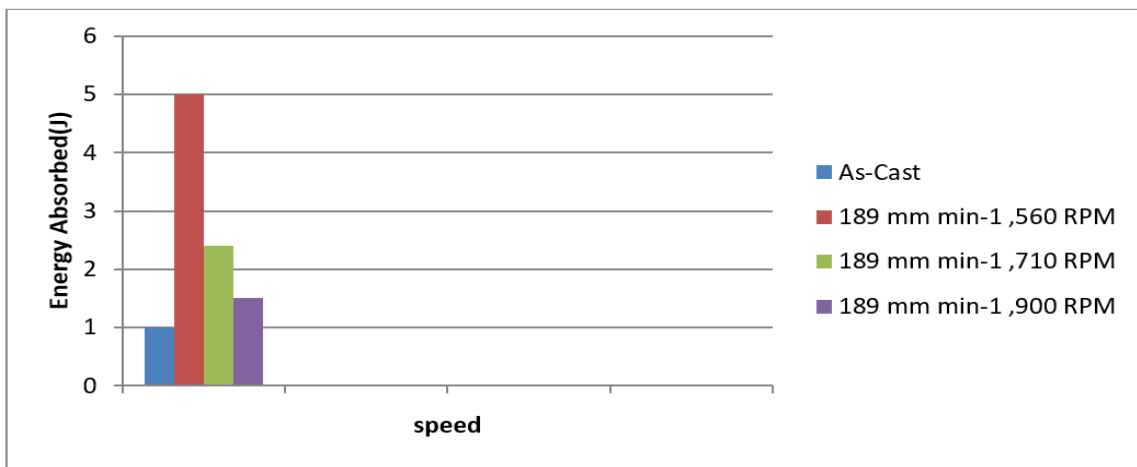


Figure 13. Influence of tool speed on the impact energy absorbed by Alloy-3 PZ after FSP.

3.6. Hardness test results

Table 10 lists the alloys' respective hardness values. Alloy-1 has the lowest hardness (52 HV) among the cast Al-Si alloys, whereas Alloy-2 has a slightly larger hardness (64 HV) because of the greater primary Si particle volume fraction. The hardest alloy was Alloy-3 (75 HV). All three alloys within the PZ exhibited minimal fluctuations in hardness after FSP. Studies have shown that improving the microstructure has little effect on the toughness of a material. Therefore, there doesn't seem to be much difference in hardness between the processed tracks [18]. Average values of the three tests representing the hardness test results for the three alloys are shown in Figures 14-18.

Examples of the hardness profiles at different rotation speeds from Alloy-1 to FSP throughout the PZ are summarized in Figure 12. This behavior is unusual in nonheat-treatable alloys, which typically exhibit improved hardness as a result of microstructure refinement [12]. It can be shown that Hall-Petch hardening has very little effect on the pure Al cast and the Al-Si cast alloys, despite the fact that the grains were significantly refined following FSP.

Table 10. Average hardness values of the as-cast alloys

Material	Alloy-1	Alloy-2	Alloy-2
Hardness (HV)	52	64	75

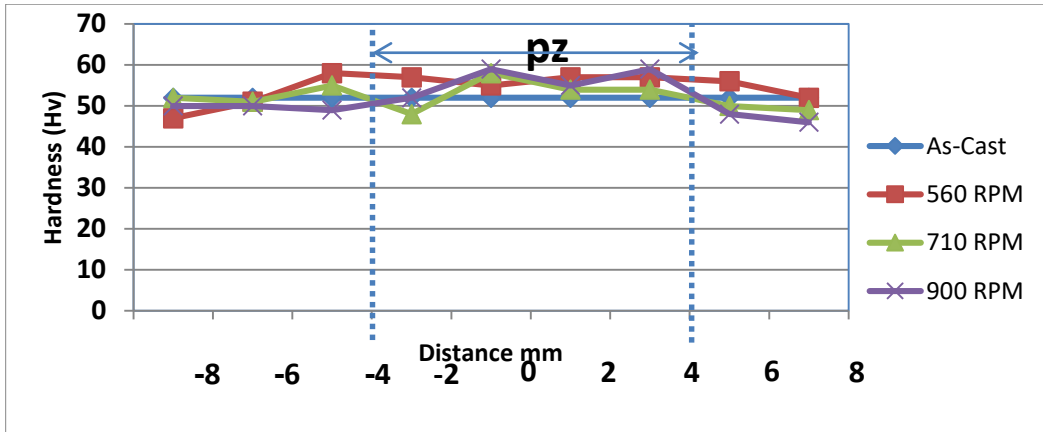


Figure 14. Profiles of hardness in the PZ from alloy-1 to (FSP) at a speed of transverse 86 mmmin⁻¹ and accelerated speed of rotation.

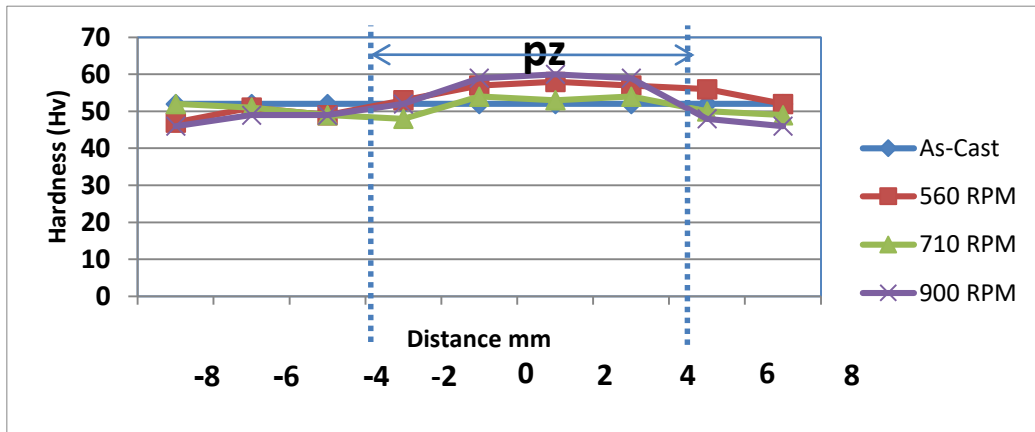


Figure 15. Hardness profiles in PZ from alloy-1 to (FSP) a rotating rise rate with 189 mmmin⁻¹ a speed of transverse.

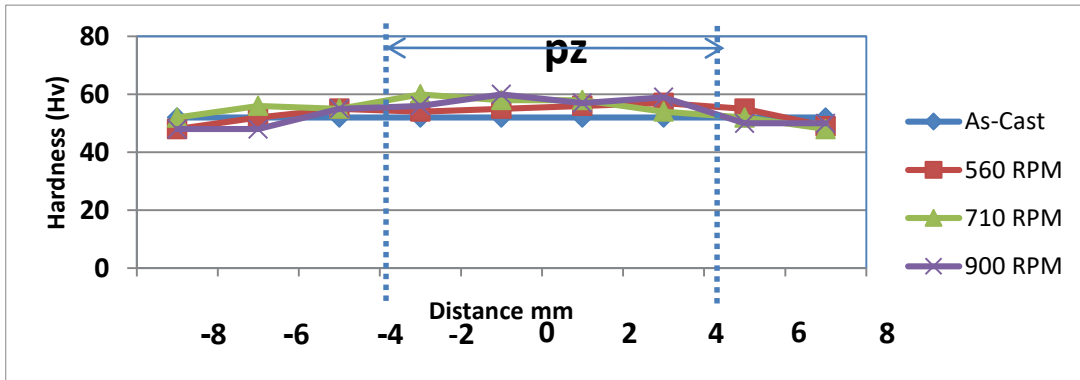


Figure 16. Hardness profiles in PZ from alloy-1 to (FSP) at a rotating rise rate a with a speed of transverse of 393 mm/min.

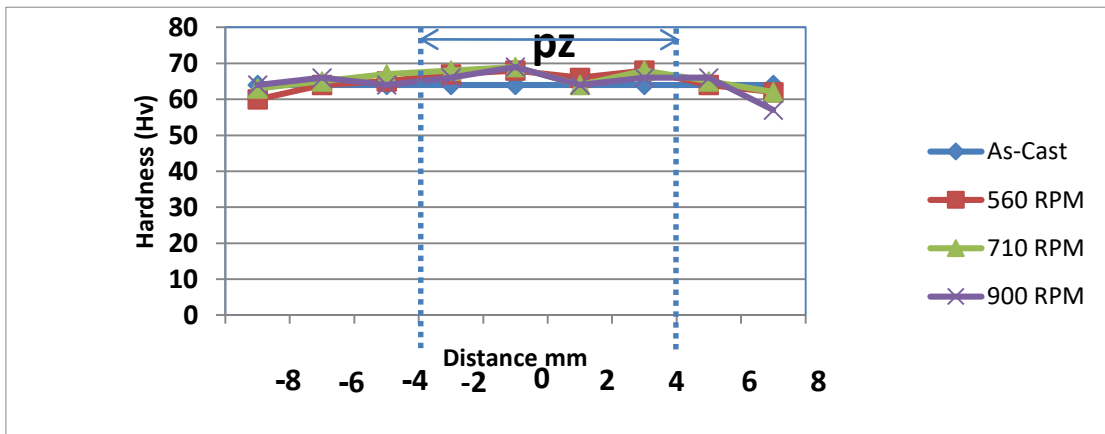


Figure 17. Hardness profiles in PZ for alloy-2 to FSP at rotating rise rate with speed of transverse of 189 mm/min

3.7. Temperature distribution

The IR camera, which has software for analyzing image of the thermal for treatment zone, recorded temperature distributions during the FSP. Processing line runs parallel to the temperature profile. The temperature range of the camera, which is 0 °C to 270 °C, as shown in Figures 19 and 20, led to the selection of points (A) and (B) for recording the peak temperature. The peak temperatures at (A) and (B) are shown in the results based on the various conditions listed below.

1. The tool shoulder plunging depth is 0.25 mm, and the tool tilting angle is 2°.
2. The rotation speeds of the tool were 560 rpm, 710 rpm and 900 rpm in the clockwise direction.
3. The travel speeds were 86, 189, and 393 mm/min.

Increasing the speed (560 to 900 rpm) is expected to result in an increase in peak processing temperature by approximately 40 °C because of increased friction between the tool surface and the machined metal. After a residence time of approximately 30 seconds during the FSP, the peak temperatures recorded from point (A) are shown in Figure 21. At a constant rotation speed of 560 rpm, speed of the transverse was decrease from (393 to 86 mm/min). Since

the 86 mmmin-1 cross-speed has a maximum temperature approximately 63 °C higher than the 393 mm/min cross-speed, the peak temperature increases as the cross-speed is reduced, as shown in Figure 22. Figure 23 shows that the temperature on the forward side was larger than that on the return side under all the conditions applied [27]-[28].

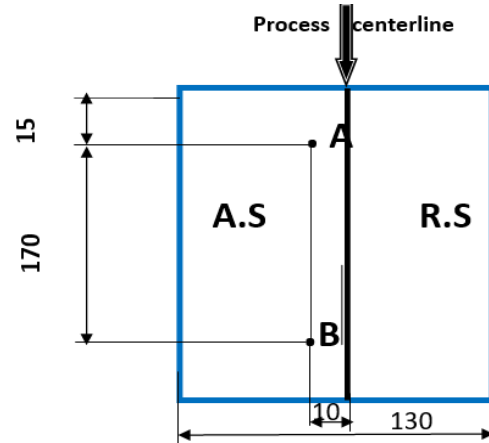


Figure 19. A and B points on the processed plate (dimensions are in mm).

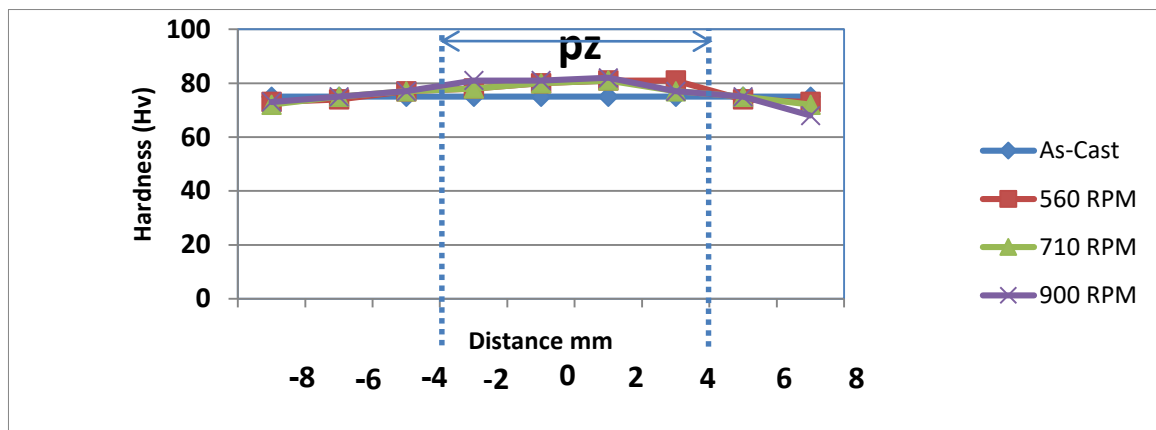


Figure 18. Hardness profiles in the entire PZ from Alloy-3 to FSP at a rotating rise rate and a 189 mm/min transverse speed.

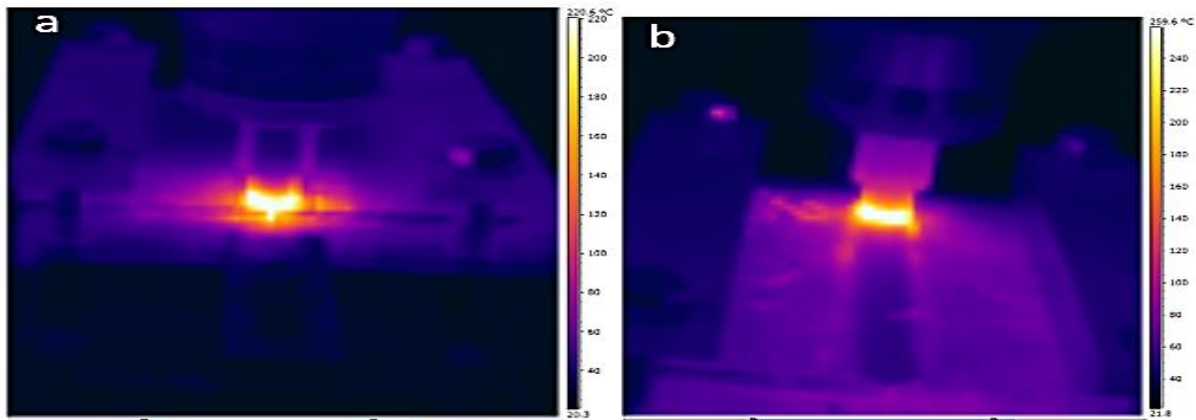


Figure 20. Thermal image. (a) Thermal image at point A. (b) Thermal image at point B.

3.8. Phases Identification

The XRD results shown in Figure 24 reveal that the hypoeutectic, eutectic, and hypereutectic Al-Si alloys

develop similar phases due to the similar chemical compositions of the alloys. In addition to the Al matrix, Si is the main phase of the alloys. The phases of the structure before and after FSP appear to be identical.

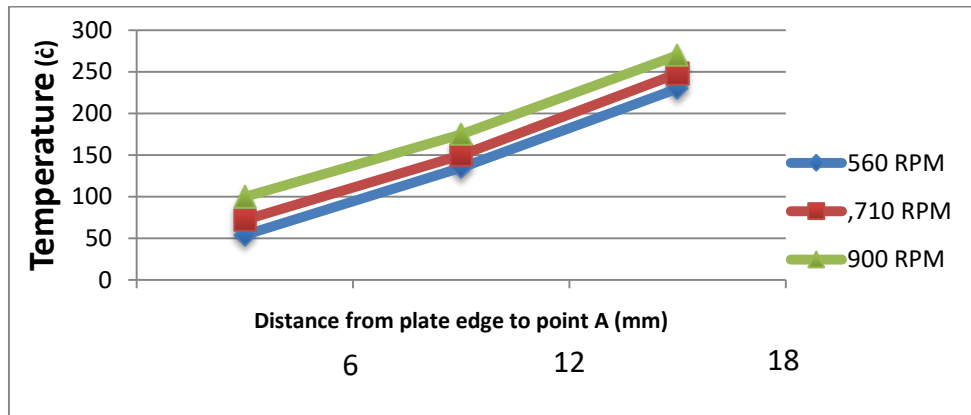


Figure 21. Peak temperature at point (A) at three rotation speeds.

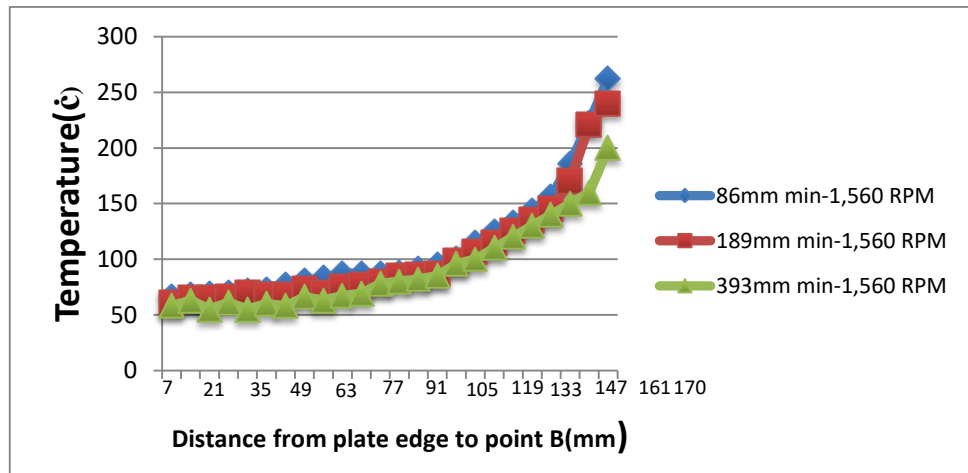


Figure 22. Peak temperature at point (B) at three transverse speeds.

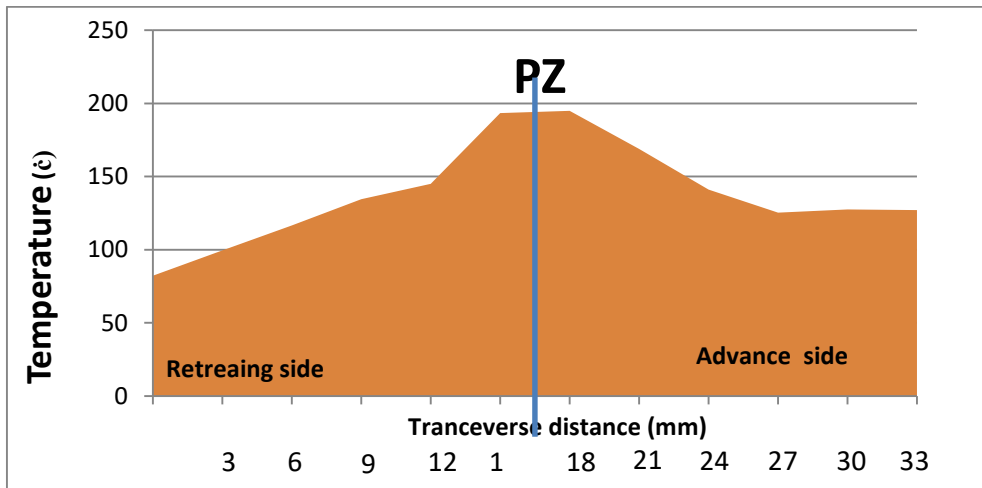


Figure 23. Temperature distributions on sides of the advancing and retreating for all the conditions employed.

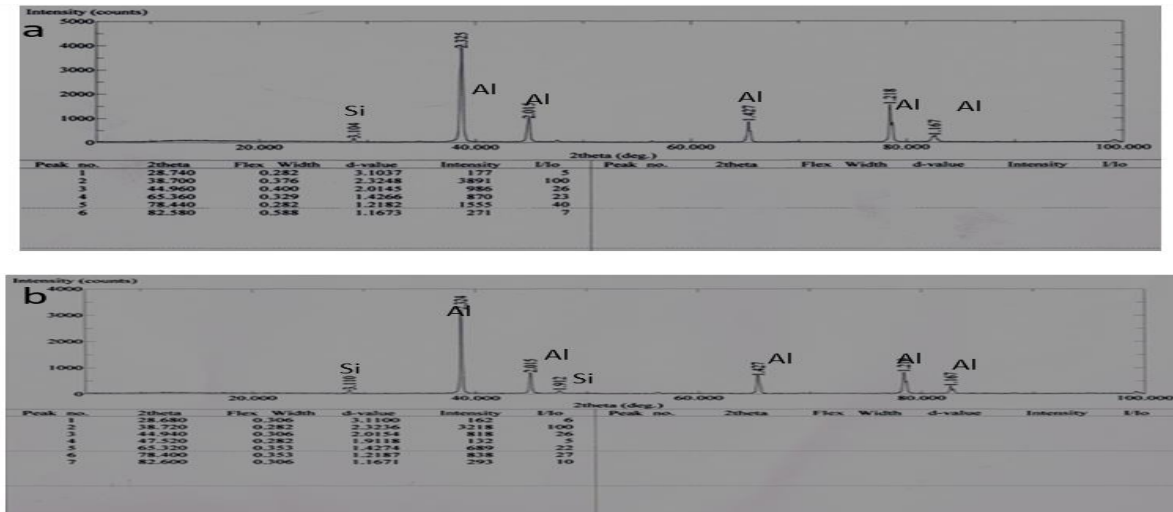


Figure 24. XRD patterns (a) before FSP and (b) after FSP (Alloy-1), with the identified phases shown

Conclusion

This study addresses the mechanisms underlying grain refinement during fine structure precipitation (FSP) of aluminum-silicon cast alloys and the effects of changes processing parameters on this process. Below, you will find a summary of the most important results.

- Microstructure of aluminum-silicon cast alloys greatly improved following FSP. In general, the advancing side outperformed the retracting PZ in terms of grain distribution and refinement when the tool rotation speed was low.
- The PZ developed a cross-sectional basin geometry that grew narrower toward the base of the PZ and was widest at the surface. The cast Al-Si alloys had incredibly poor tensile properties, as demonstrated by tensile tests. However, the material's ductility following FSP increased dramatically because the large Si particles that were prone to cracking were refined and the voids in the microstructure were eliminated.
- Compared with those of the matching base metals, the impact energies of the FSP material were greater.
- The temperature decreases at less speeds of rotational and large speeds of transverse, which decreases the softening effect of the tool as it moves through the material.
- Temperature distribution on the advancing and retreating sides, with the advancing side recording a higher peak temperature.
- An the material hardness did not significantly change after FSP.

References

- [1] Kamlesh Meena, Aditya Kumar, Shailesh N. Pandya, "Optimization of Friction Stir Processing Parameters for 60/40 Brass using Taguchi Method". Volume 4, Issue 2, Part A, 2017, PP. 1978-1987.
- [2] R.S. Mishra, Z.Y. Ma, and I. Charit, "Friction stir processing: a novel technique for fabrication of surface composite", Mater. Sci. Eng., vol. A341, 2003, pp. 307-310.
- [3] P.B. Berbon, W.H. Bingel, R.S. Mishra, C.C. Bampton, and M.W. Mahoney, "Friction stir processing: a tool to homogenize nanocomposite aluminum alloys", Scripta Mater., vol. 44, 2001, pp. 61-66.
- [4] Z.Y. Ma, S.R. Sharma, R.S. Mishra, and M.W. Mahoney, "Microstructural modification of cast aluminum alloys via friction stir processing", Mater. Sci. Forum, vols. 426-432, 2003, pp. 2891-2896.
- [5] Y. K. Yousif, K. M. Daws, B. I. Kazem, "Prediction of Friction Stir Welding Characteristic Using Neural Network", Jordan Journal of Mechanical and Industrial Engineering, Volume 2, 2008, Pages 151 - 155.
- [6] Vaibhav S. Gaikwad, Satish S. Chinchankar, "Adaptive Neuro Fuzzy Inference System to Predict the Mechanical Properties of Friction Stir Welded AA7075-T651 Joints", Jordan Journal of Mechanical and Industrial Engineering, Volume 16, 2022, Pages 381-393.
- [7] G. C. Tejaswini, B. Lathashankar, R. Suresh, Gowtham Venkatesan, N.G. Siddesh Kumar, "Investigation on Effect of Temperature on Mechanical Properties and Microstructure of Dissimilar Ti-5Al-2.5Sn and AA2219 Alloy Joints through Diffusion Bonding Process", Jordan Journal of Mechanical and Industrial Engineering, Volume 8, 2024, Pages 891- 899.
- [8] A.H.Q. Ayun, J. Triyono, E. Pujiyanto, "Optimization of Injection Molding Simulation of Bioabsorbable Bone Screw Using Taguchi Method and Particle Swarm Optimization", Jordan Journal of Mechanical and Industrial Engineering, Vol. 16, No. 2, 2022, pp. 319-325.
- [9] AKe Qiao, Ting Zhang, Kuaishe Wang, Shengnan Yuan etc., "Mg/ZrO₂ Metal Matrix Nanocomposites Fabricated by Friction Stir Processing: Microstructure, Mechanical Properties, and Corrosion Behavior", Front Bioeng Biotechnol. 2021 9, 605171.
- [10] F. B. Ismail, A. Al-Bazi, R. H. Al-Hadeethi, M. Victor, "A Machine Learning Approach for Fire-Fighting Detection in the Power Industry". Jordan Journal of Mechanical and Industrial Engineering, Vol. 15, No. 5, 2021, pp. 475-482.
- [11] Manh Tien Nguyen, Truong An Nguyen, Duc Hoan Tran and Van Thao Le, "Optimization of Superplastic Forming Process of AA7075 Alloy for the Best Wall Thickness Distribution", AITI ranks, Vol. 6, 2021, No. 4.
- [12] Yu-lu Duan, Jian Qian, Dan Xiao, Xue-min Cui & Guo-fu Xu, "Effect of Sc and Er additions on superplastic ductility's in Al-Mg-Mn-Zr alloy", Materials, Metallurgy, Chemical and Environmental Engineering, Volume 23, 2016, pages 1283-1292.
- [13] Uday Sen and Kulbhushan Sharma, "Effects of Process Parameters of Friction Stir Processing on Tensile Strength of AA6063 Aluminum Alloy", International Journal of Scientific Research in Science, Engineering and Technology, Vol. 2 No. 2 .2016.

- [14] Mohamed EL.Sayed A.Y., Mohamed A. EL-Nikhaily, "Effect of friction stir processing on the mechanical properties and microstructure of cast aluminum (Al-Si-Zn-Cu) Alloy", *Engineering research journal*, 137, 2013.
- [15] Quan Liu, Xiaomi Chen, KunLiu, Valentino A. M. Cristiano, Kin-Ho Lo, Zhengchao Xie, Dawei Guo, Lap-Mou Tam and Chi-Tat Kwok, "Influence of Processing Parameters on Microstructure and Surface Hardness of Hypereutectic Al-Si-Fe-Mg Alloy via Friction Stir Processing", *Coatings*, 14, 2024, 222.
- [16] L. John Baruch, R. Raju, V. Balasubramanian, A. G. Rao, I. Dinaharan, "Influence of Multi-pass Friction Stir Processing on Microstructure and Mechanical Properties of Die Cast Al-7Si-3Cu Aluminum Alloy", *Acta Metall. Sin.*, 29(5), 2016, 431-440.
- [17] Ma, Z.Y., Sharma, S.R., Mishra, R.S. "Effect of multiple-pass friction stir processing on microstructure and tensile properties of a cast aluminum-silicon alloy", *Scripta Materialia*, vol. 54, 2006, pp. 1623-1626.
- [18] E. N. Ryl'kov, F. Yu. Isupov, A. A. Naumov, O. V. Panchenko & A. I. Shamshurin, "Microstructure and Mechanical Properties of Dissimilar Al-Cu Joints Formed by Friction Stir Welding", *Metal Science and Heat Treatment* Volume 60, 2019, pages 734-738.
- [19] Chun Yip Chan, "Friction stir processing of aluminum-silicon alloys". a thesis submitted to the University of Manchester for the degree of doctor of philosophy in the faculty of engineering and physical sciences. 2011.
- [20] Ahmad Mostafa, and Nabeel Alshabat, "Microstructural, Mechanical and Wear Properties of Al-1.3%Si Alloy as Compared to Hypo/Hyper-Eutectic Compositions in Al-Si Alloy System", *Crystals* 12(5), 2022, 719.
- [21] Santella, M.L., Engstrom, T., Storjohann, D., Pan, T.-Y. "Effects of friction stir processing on mechanical properties of the cast aluminum alloys A319 and A356", *Scripta Materialia*, vol. 53, 2005, pp. 201-206.
- [22] Ma, Z.Y., Sharma, S.R., Mishra, R.S. "Effect of Friction stir processing on the microstructure of cast A356 aluminum", *Materials Science and Engineering A*, 433, 2006, pp. 269-278.
- [23] Seidel, T.U., Reynold, A.P. "Visualization of the material flow in AA2195 friction-stir welds using a marker insert technique", *Metallurgical and Materials Transactions A*, 32, 2001, pp. 2879-2884.
- [24] P. Ning, "An adaptive scheduling method for resources in used automobile parts recycling". *Jordan Journal of Mechanical and Industrial Engineering*, Vol. 14, No. 1, 2020, pp. 53-60.
- [25] Ahmed R. S. Essa, Ramy I. A. Eldersy, Mohamed M. Z. Ahmed, "Modeling and Experimental Investigation of the Impact of the Hemispherical Tool on Heat Generation and Tensile Properties of Dissimilar Friction Stir Welded AA5083 and AA7075 Al Alloys", *Materials*, 17(2), 2024, pp. 433.
- [26] Lee, M.H., Kim, J.J., Kim, K.H., Kim, N.J., Lee, S., Lee, E.W. "Effects of HIPping on high-cycle fatigue properties of investment cast A356 aluminum alloys", *Materials Science and Engineering A*, 340, 2003, pp. 123-129.
- [27] Arul Oli P. J, Sriviniyaga and Parthasarathy. "Friction stir welding of dissimilar aluminum alloys AA7075 to AA2014.", *International Journal of Health Sciences* Vol. 6, 2022, No. S4.
- [28] M. Soori, M. Asmael, "A Review of the Recent Development in Machining Parameter Optimization". *Jordan Journal of Mechanical and Industrial Engineering*, Vol. 16, No. 2, 2022 pp. 205-223.